Proceedings of IMECE'03
2003 ASME International Mechanical Engineering Congress & Exposition
November 16-21, 2003, Washington, D.C. USA

IMECE2003-42542

LOCAL SPACE-TIME ADAPTIVE DISCONTINUOUS GALERKIN FINITE ELEMENT METHODS FOR TIME-DEPENDENT WAVES

Lonny L. Thompson* **and Dantong He**
Advanced Computational Engineering & Mechanics Lab
Department of Mechanical Engineering
Clemson University
Clemson, South Carolina, 29634-0921
Email: lonny.thompson@ces.clemson.edu

ABSTRACT

Local space-time adaptive methods are developed including high-order accurate nonreflecting boundary conditions (NRBC) for time-dependent waves. The time-discontinuous Galerkin (TDG) variational method is used to divide the time-interval into space-time slabs, the solution advanced from one slab to the next. Within each slab, a continuous space-time mesh is used which enables local sub-time steps. By maintaining orthogonality of the space-time mesh and pre-integrating analytically through the time-slab, we obtain an efficient yet robust local space-time adaptive method. Any standard spatial element may be used together with standard spatial mesh generation and visualization methods. Recovery based error estimates are used in both space and time dimensions to determine the number and size of local space-time elements within a global time step such that both the spatial and temporal estimated error is equally distributed throughout the space-time approximation. The result is an efficient and reliable adaptive strategy which distributes local space-time elements where needed to accurately track time-dependent waves over large distances and time. Numerical examples of time-dependent acoustic radiation are given which demonstrate the accuracy, reliability and efficiency gained from this new technology.

*Corresponding Author

INTRODUCTION

For wave modeling, a standard approach is to use explicit methods which do not require matrix factorization to advance solutions in time at discrete time-steps. However, a difficulty with these methods is that they are only conditionally stable, requiring a small time step below a limit dictated by the size of the smallest elements in a discretization of the computational domain. Often for unstructured and adaptive meshes for complex structures, there may be a small number of patches in a mesh with relatively small element size compared to the majority of larger elements in other regions. To ensure reliability, a smaller time step than required for accuracy is often used, resulting in a potentially inefficient solution. For example, a sufficiently accurate solution may be obtained with 20 time-steps per wave period, yet to ensure stability throughout the entire mesh, often the time-step requirement is run at over 100 time-steps per wave period, resulting in a large number of time steps to advance the solution over large time-intervals found in many applications including radiation and scattering of acoustic and elastodynamic waves.

Unconditionally stable implicit time-stepping methods commonly used in structural dynamics such as the Newmark and related family of second-order methods exhibit significant dispersion and or amplitude decay errors for wave pulses with broadband frequencies traveling over large distances and time, causing misrepresentation of arrival time and directionality at a distant target. To minimize these errors, higher-order accurate methods are needed. Time-discontinuous Galerkin (TDG) finite element methods employ finite element discretization of the time domain

as well as the usual discretization of the spatial domain, [1]- [13], and provide a foundation on which to built high-order accurate and adaptive time-stepping methods. TDG methods are characterized by allowing for discontinuous solutions at the beginning of each time step.

In this work we propose high-order accurate and unconditionally stable TDG space-time finite element methods with the ability to adaptively distribute local sub-time steps for different elements in an adaptive spatial mesh in order to reliably and efficiently track localized waves over large distances and time.

In [11]- [14], comprehensive adaptive procedures for a multi-field TDG space-time finite element method including high-order accurate nonreflecting boundary conditions for unbounded wave problems were developed. The solution method used a multi-level iterative solver for the coupled interior/boundary equation system built from independent displacement and velocity field variables together with auxiliary functions appearing in nonreflecting boundary conditions for wave problems in unbounded domains. The adaptive methods were demonstrated for the scalar wave equation in two spatial dimensions with independent pressure and velocity potential field variables in the TDG-FEM for acoustic radiation and scattering problems. The TDG-FEM formulation for acoustic variables was first given in [7, 8].

An *h*-adaptive space-time strategy was employed based on the Zienkiewicz-Zhu [17] spatial error estimate using the superconvergent patch recovery (SPR) technique for the spatial mesh at the end of a time-step. Using this adaptive strategy, as wave pulses propagate throughout the mesh, elements are refined near wave fronts, and unrefined where the solution is smooth or quiescent, providing efficient wave tracking over large distance and time.

In [9], [11]- [13], [14], a global time-stepping strategy was used based on measuring the jump, i.e., the difference in the discontinuous solution at each time-step measured in an energy norm. The effectiveness of the jump in discontinuous solutions as an error indicator was shown in [14] to be due to the superconvergent property of the TDG solution at the end of a time-step. A limitation of this previous work was that while the global time step size could be adjusted to maintain a given estimated error tolerance, the same time step size had to be used for every spatial element in the computational domain. In this work, a generalization of the above strategy to include the use of local sub-time step sizes for each spatial element is developed. Similar to the adaptive distribution of spatial elements, for localized wave pulses propagating throughout the computational domain, elements near wave fronts will have small sub-time step sizes within a global space-time slab in the TDG-FEM. Fewer, sub-time steps are used where the solution is smooth or quiescent, providing improved efficiency in tracking localized waves over large distances and time.

Adaptive time-stepping methods require projection methods to transfer solutions from a previous mesh to a current mesh. For low-order elements, standard nodal interpolation may lead to significant accumulation of error over time. To minimize this difficulty, a new superconvergent interpolation (SI) method developed in [14] will be used in this work.

The most general strategy is to treat the time-domain as another dimension on par with the spatial dimensions. For example, for a problem in two space dimensions, the time dimension would create an unstructured mesh of three-dimensional space-time elements such as hexahedra or tetrahedra within a space-time slab. In this strategy, there is no distinction between space and time, and an unstructured three-dimensional space-time mesh could be used. A difficulty with this approach is that for problems in three spatial dimensions, the fourth time-dimension on unstructured space-time element meshes requires special 4-dimensional elements to be formulated with complicated Jacobian transformations to a four-dimensional reference element, and requires special 4-dimensional mesh generation and visualization schemes.

A slightly more restrictive yet greatly simplified strategy proposed here is to limit the local space-time elements within a mesh to be orthogonal with respect to space and time. In this strategy element edges in the time direction remain orthogonal to the spatial dimension. This results in an uncoupled space-time element Jacobian transformation. As a result, the integration over a local sub-time step is independent of the spatial coordinates and thus can be evaluated analytically in closed-form for each element. This has the advantage that any standard spatial element may be used; the time integration carried out independently. For example, for structural acoustics problems, standard acoustic and shell elements may be used.

While solutions remain discontinuous at the beginning of a global space-time slab, local space-time elements are continuous within the global slab. Our approach could then be described as a mixed Time-Discontinuous Galerkin (TDG) method for global time-stepping with local continuous approximation within a global step. To match continuity in time for adjacent space-time elements, transition elements with a single mid-edge node in the time-dimension are developed to connect elements with different sub-time step sizes. Other standard approaches may be used to enforce continuity, including constraint conditions used in hp-FEM. In contrast to an unstructured space-time mesh strategy, the strategy of maintaining orthogonality of space and time enables the straightforward implementation of problems in both two- and three- spatial dimensions. No special four-dimensional mesh generators or complicated visualization techniques are required.

When introducing local sub-time steps for different elements within a global space-time slab, the temporal error estimator based on the difference (jump) in solutions between time slabs used in our previous work proved unreliable. In order to obtain an effective temporal error estimator three alternatives are pro-

posed. In the first, the temporal error estimator is based on the difference between the independent velocity variable v^h and the time-derivative of the displacement variable du^h/dt. In the second, the recovered temporal derivatives using the superconvergent patch recovery (SPR) technique are compared to the lower order finite element approximation to the time derivative. The third approach uses the SPR recovered time-derivatives with the superconvergent interpolation (SI) method applied in the time dimension to obtain improved temporal solutions. This superconvergent interpolation uses the more accurate recovered time-derivatives to obtain more accurate solutions within an element. Based on the local temporal error estimates within each element, a local temporal h-adaptive strategy is proposed to redistribute sub-time steps such the error is approximately equally distributed. When a given temporal error tolerance is exceeded, the error is redistributed by using more sub-time steps in elements with large temporal errors.

The assembled coupled interior/boundary equation system is solved using a restarted Generalized Minimal Residual (GMRES) iterative solver [19] with Incomplete Lower-Upper factorization with dual truncation (ILUT) [20] preconditioning. A simpler Jacobi preconditioner is used for the boundary equations. To accurately model the unbounded region, the high-order local radiation boundary conditions (RBC) derived in Hagstrom and Hariharan [15, 16] are applied on an artificial truncated boundary; here implemented with the TDG-FEM.

Exterior Acoustic Wave Problem

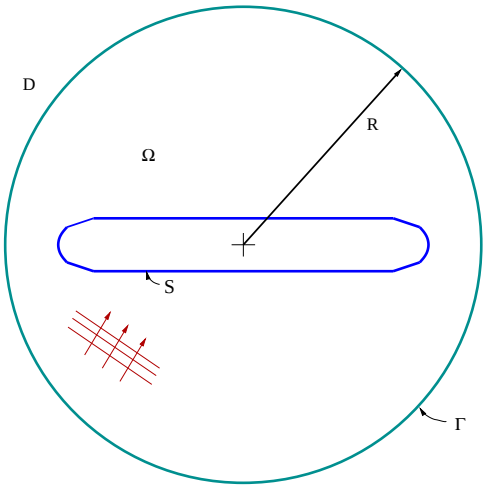

Figure 1. Illustration of two-dimensional unbounded region R surrounding a scatterer S. The computational domain $\Omega \subset R$ is surrounded by a circular truncation boundary Γ of radius R, with exterior region $D = R - \Omega$.

Consider time-dependent waves in an infinite two-dimensional region R, surrounding an object with surface S. For computation, the unbounded region is truncated by an artificial circular boundary Γ, of radius $||\boldsymbol{x}|| = R$, resulting in a finite domain $\Omega \subset R$, see Figure 1. Within Ω, the solution $u(\boldsymbol{x},t)$, satisfies the scalar wave equation with wave speed $c > 0$,

$$\frac{1}{c^2}\frac{\partial v}{\partial t} = \nabla^2 u + f(\boldsymbol{x},t), \qquad v = \frac{\partial u}{\partial t}, \qquad \boldsymbol{x} \in \Omega,\ t > 0 \tag{1}$$

with initial conditions, $u(\boldsymbol{x},0) = u_0(\boldsymbol{x}), v(\boldsymbol{x},0) = v_0(\boldsymbol{x})$. The source f and initial data u_0 and v_0 are assumed to be confined to the computational domain Ω, so that in the exterior region $D = R - \Omega$, the scalar field $u(\boldsymbol{x},t)$ satisfies the homogeneous form of the wave equation. For acoustics, u may be considered the pressure fluctuation from a reference state. Assuming linear irrotational fluids, u may also represent a velocity potential field. To specify radiation or scattering directly on the surface S, a Neumann boundary condition is specified,

$$\frac{\partial u}{\partial n} = g(\boldsymbol{x},t), \qquad \boldsymbol{x} \in S,\ t > 0 \tag{2}$$

In linear acoustics, the condition $g = 0$, corresponds to a 'rigid' scatterer. For later use, the solution evaluated on the circular truncation boundary at $r = R$, is denoted by, $u_\Gamma(\theta,t) = u(R,\theta,t),\ \theta \in [0,2\pi),\ t > 0$, Similarly, $v_\Gamma(\theta,t) = \partial u_\Gamma/\partial t$.

Let $\boldsymbol{w}(\theta,t) = \{w_j(\theta,t)\}_{j=1}^{p}$, be defined as a time-dependent vector of p, real valued scalar auxiliary functions. We then define a sequence of high-order accurate local radiation boundary conditions (RBC) on the artificial truncation boundary Γ, by [16]

$$\left.\frac{\partial u}{\partial r}\right|_{r=R} + \frac{1}{c}v_\Gamma(\theta,t) + \frac{1}{2R}u_\Gamma(\theta,t) = \frac{1}{R}w_1(\theta,t) \tag{3}$$

The boundary function $w_1(\theta,t)$ is the first coefficient in the vector $\boldsymbol{w}$, and is found by solving the following first-order partial differential equation system in time: Given $u_\Gamma(\theta,t)$, Find $\boldsymbol{w}(\theta,t)$, such that,

$$\frac{1}{c}\frac{\partial \boldsymbol{w}}{\partial t} + \frac{1}{4R}\left(\boldsymbol{A}_1 + \boldsymbol{A}_2\frac{\partial^2}{\partial\theta^2}\right)\boldsymbol{w}(\theta,t) = \boldsymbol{b}\,u_\Gamma(\theta,t), \tag{4}$$

In the above, $\boldsymbol{A}_1$ and $\boldsymbol{A}_2$ are constant $p \times p$, tri-diagonal and uni-diagonal matrices, respectively, defined with band:

$$\begin{aligned}\boldsymbol{A}_1 &= \text{Band}\left[-(j-\frac{1}{2})^2,\, 4j,\, -4\right];\\ \boldsymbol{A}_2 &= \text{Band}\left[-1,\, 0,\, 0\right].\end{aligned} \tag{5}$$

The vector operator,

$$\boldsymbol{b} = \frac{1}{R}\left(b_1 + b_2\frac{\partial^2}{\partial\theta^2}\right)\boldsymbol{e}_1, \qquad b_1 = 1/8, \quad b_2 = 1/2 \tag{6}$$

is defined by $\boldsymbol{e}_1 = \{\delta_{j1}\}_{j=1}^{p}$; the scaled unit vector of order p. In the above, the recursive sequence has been scaled by $\{w_j\} = \{R^j z_j\}$, where $\{z_j\}$ are the original boundary functions derived in [15]. This rescaling renders the coefficient matrices $\boldsymbol{A}_1$ and $\boldsymbol{A}_2$ to be independent of R. Since both (3) and (4) contain the boundary functions $w_1(\theta,t)$ and $u_\Gamma(\theta,t)$, the equations (1) and (4) are coupled. This sequence of boundary conditions have been implemented in [16] and shown to be increasingly accurate as the number of functions p is increased.

TDG FEM Formulation with Local RBC

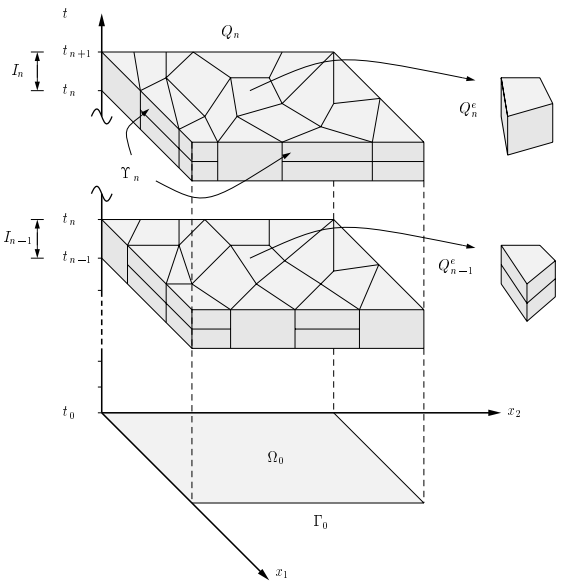

Figure 2. Illustration of two consecutive space-time slabs showing local sub-time steps within different space-time elements.

The development of the space-time method proceeds by considering a partition N of the total time interval, $t \in J = (0,T), 0 < T < \infty$, of the form: $0 = t_0 < t_1 < \cdots < t_N = T$, into N time steps $\{I_n\}_{n=0}^{N-1}$ given by $I_n = \{(t_n, t_{n+1})\}$. The length of the variable time step is given by $\Delta t_n = t_{n+1} - t_n$. Using this notation, $Q_n = \Omega \times I_n$, are the nth space-time slabs. Figure 2 shows an illustration of two consecutive space-time slabs Q_{n-1} and Q_n, each with different meshes. Within each space-time element, the trial solution and weighting function are approximated by a finite basis which depend on both spatial $\boldsymbol{x}$, and temporal t, dimensions. The basis functions are assumed $C^0(Q_n)$ continuous throughout each space-time slab, but are allowed to be discontinuous across the interfaces of the slabs. The space of finite element basis functions in a multi-field representation is stated in terms of *independent* variables u, and v, [7,8].

In the following, the space-time finite element formulation for the initial-boundary value problem within the bounded computational region $Q_n = \Omega \times I_n$, supplemented by the local radiation boundary conditions (RBC) given in (3) and (4) on $\Gamma \times I_n$, is given. The statement of the time-discontinuous Galerkin (TDG) method may be stated as, *Given:* source and boundary data f, g, and initial conditions $\{u(\boldsymbol{x},t_n^-), v(\boldsymbol{x},t_n^-)\}$, and $\boldsymbol{w}(\theta,t_n^-)$, projected from the previous time step, then for each space-time slab, $n = 0,1,\ldots,N-1$; *Find:* $\boldsymbol{u} = \{u(\boldsymbol{x},t), v(\boldsymbol{x},t)\}$, and $\boldsymbol{w}(\theta,t)$, where $\boldsymbol{x} \in \Omega \cup \partial\Omega$, $t \in I_n = (t_n, t_{n+1})$, and $\theta \in (0, 2\pi)$, such that for all admissible functions $\bar{\boldsymbol{u}} = \{\bar{u}(\boldsymbol{x},t), \bar{v}(\boldsymbol{x},t)\}$, and $\bar{\boldsymbol{w}}(\theta,t)$, the following coupled variational equations are satisfied,

$$A(\bar{\boldsymbol{u}}, \boldsymbol{u})_n + B_\Gamma(\bar{\boldsymbol{u}}, \boldsymbol{u})_n = F_S(\bar{v})_n + F_\Gamma(\bar{v}, w_1)_n \tag{7}$$

$$A_\Gamma(\bar{\boldsymbol{w}}, \boldsymbol{w})_n = F_\Gamma(\bar{\boldsymbol{w}}, u)_n \tag{8}$$

In the above,

$$A(\bar{\boldsymbol{u}}, \boldsymbol{u})_n := \int_{I_n}\left\{(\bar{v}, \frac{1}{c^2}\frac{\partial v}{\partial t}) + (\nabla\bar{v}, \nabla u) + (\nabla\bar{u}, \nabla\frac{\partial u}{\partial t} - \nabla v)\right\} \mathrm{d}t + (\bar{v}(t_n^+), [\![\frac{1}{c^2}v(t_n)]\!]) + (\nabla\bar{u}(t_n^+), [\![\nabla u(t_n)]\!]) \tag{9}$$

$$B_\Gamma(\bar{\boldsymbol{u}}, \boldsymbol{u})_n := \int_{I_n}\left\{\frac{1}{c}(\bar{v}, v)_\Gamma + \frac{1}{2R}(\bar{v}, u)_\Gamma + \frac{1}{2R}(\bar{u}, \frac{\partial u}{\partial t} - v)_\Gamma\right\} \mathrm{d}t + \frac{1}{2R}(\bar{u}(t_n^+), [\![u(t_n)]\!])_\Gamma \tag{10}$$

$$F_S(\bar{v})_n := \int_{I_n}\{(\bar{v}, f) + (\bar{v}, g)_S\}\ \mathrm{d}t \tag{11}$$

$$A_\Gamma(\bar{\boldsymbol{w}}, \boldsymbol{w})_n = \int_{I_n}\left\{\frac{1}{c}(\bar{\boldsymbol{w}}, \frac{d\boldsymbol{w}}{dt})_\Gamma + (\bar{\boldsymbol{w}}, \boldsymbol{A}\boldsymbol{w})_\Gamma\right\} \mathrm{d}t + \frac{1}{c}(\bar{\boldsymbol{w}}(t_n^+), [\![\boldsymbol{w}(t_n)]\!])_\Gamma \tag{12}$$

$$F_\Gamma(\bar{v}, w_1)_n = \int_{I_n}(\bar{v}, w_1)_\Gamma\ \mathrm{d}t \tag{13}$$

$$F_\Gamma(\bar{\boldsymbol{w}}, u)_n = \int_{I_n}(\bar{\boldsymbol{w}}, \boldsymbol{b}u)_\Gamma\ \mathrm{d}t \tag{14}$$

Integration is taken over a typical time interval $I_n = (t_n, t_{n+1})$, with size $\Delta t_n = (t_{n+1}^- - t_n^+) > 0$. The parenthesis notation $(\cdot,\cdot)$, denotes a standard integral (L_2 inner product) defined over Ω. In the above, integration-by-parts on the boundary is used to balance the angular derivatives appearing in the local boundary op-

erators,

$$(\bar{\boldsymbol{w}},\boldsymbol{A}\,\boldsymbol{w})_\Gamma = \frac{1}{4R}(\bar{\boldsymbol{w}},\boldsymbol{A}_1\,\boldsymbol{w})_\Gamma - \frac{1}{4R}(\frac{\partial\bar{\boldsymbol{w}}}{\partial\theta},\boldsymbol{A}_2\,\frac{\partial\boldsymbol{w}}{\partial\theta})_\Gamma \qquad (15)$$

$$(\bar{\boldsymbol{w}},\boldsymbol{b}\,u)_\Gamma = (\bar{\boldsymbol{w}},\boldsymbol{b}_1\,u)_\Gamma - (\frac{\partial\bar{\boldsymbol{w}}}{\partial\theta},\boldsymbol{b}_2\,\frac{\partial u}{\partial\theta})_\Gamma \qquad (16)$$

Local Space-Time Discretization

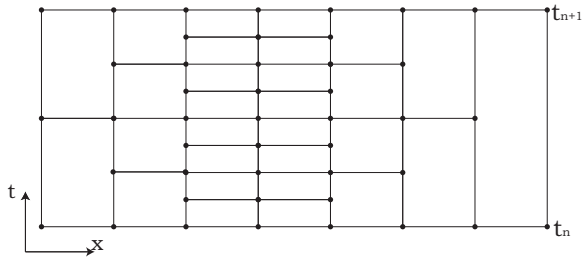

Figure 3. Illustration of local space-time elements within a time slab for one spatial dimension. The example shows a maximum of eight sub-time steps with transitions to four, then two, then one sub-time step.

To maintain decoupling of the space-time dimensions, an orthogonal space-time finite element discretization is assumed within a space-time slab $Q_n = \Omega \times I_n$. As shown in Figure 2, we first discretize the space-time domain Q_n into space-time columns based on spatial elements, then divide some of these columns with smaller sub-time steps. At a spatial element Ω^e_n, there are N^e_t non-overlapping sub-time steps with intervals,

$$I^e_{n,i} = (t^e_{n,i}, t^e_{n,i+1}),\ i = 1,\ldots,N_t$$

such that $I_n = \bigcup_{i=1}^{N^e_t} I^e_{n,i}$. With this construction, the local space-time elements are defined as $Q^e_{n,i} = \Omega^e_n \times I^e_{n,i},\ i = 1,\ldots,N^e_t$.

The local sub-time step size is defined by $\Delta t^e_{n,i} = t^e_{n,i+1} - t^e_{n,i}$, where $t^e_{n,1} = t^+_n$ and $t_{n,N^e_t+1} = t^-_{n+1}$ are the beginning and end of the global time slab. In order to simplify the discretization, all sub-time steps at one spatial element are restricted to have the same size, i.e., $\Delta t^e_n = \Delta t^e_{n,i},\ i = 1,\ldots,N^e_t$; see Figure 3. This restriction is not required in the formulation, yet will simplify the adaptive space-time mesh generation.

Within a local space-time element $\Omega^e_{n,i}$, the finite element approximation is defined as the linear combination of the usual spatial basis functions $N_a(\boldsymbol{x})$,

$$u(\boldsymbol{x},t) = \sum_{a=1}^{n_{en}} N_a(\boldsymbol{x})u_a(t) = \boldsymbol{N}^e(\boldsymbol{x})\boldsymbol{u}(t). \qquad (17)$$

In the above, $\boldsymbol{x} \in \Omega^e_n,\quad t \in I^e_{n,i} = (t^e_{n,i}, t^e_{n,i+1})$, and $a = 1,\ldots,n_{en}$ is the spatial element node number; for an element with n_{en} spatial nodes, e.g. for a triangle element with three vertices, $n_{nen} = 3$. The solution vector associated with each spatial node is $\boldsymbol{u}(t) = \{u_a(t)\}_{a=1}^{n_{en}}$. Within the ith sub-time step $I^e_{n,i}$, the time-dependent nodal solution $u_a(t)$ can be expressed with the temporal interpolation,

$$u_a(t) = \sum_{p=1}^{r_a} \phi_{a,p}(t)u_a(t_p) = \boldsymbol{\phi}_a(t)\boldsymbol{d}_a,\quad t \in I^e_{n,i} \qquad (18)$$

where $\{\phi_{a,p}(t)\}_{p=1}^{r_a}$ are time-dependent basis functions associated with spatial node a, and $\boldsymbol{d}_a = \{u_a(t_p)\}_{p=1}^{r_a}$ is the solution vector of temporal degrees-of-freedom associated with node a. The number of temporal degrees-of-freedom associated with node a is defined as r_a. Within a time-slab continuity is maintained, so that standard $C^0(I_n)$ continuous basis functions such as linear or high-order Lagrange or hierarchical interpolation functions may be used. For simplicity, we have implemented linear Lagrange interpolation; typical nodes have $r_a = 2$. Transition elements have an additional midside degrees-of-freedom along the temporal direction to allow for continuous one-half sub-time step divisions between adjacent elements.

In summary, the approximation within a space-time element $Q^e_{n,i}$, may be stated as

$$u(\boldsymbol{x},t) = \boldsymbol{N}^e(\boldsymbol{x})\boldsymbol{\phi}^e(t)\boldsymbol{d}^e \qquad (19)$$

where $\boldsymbol{\phi}^e(t)$ is an array of nodal temporal interpolation functions with partitions $\boldsymbol{\phi}_a(t)$. Here, $\boldsymbol{d}^e$ is the solution vector containing all degrees-of-freedom for the space-time element,

$$\boldsymbol{d}^e = \{u_a(t_p)\},\ a = 1,\ldots,n_{en},\ p = 1,\ldots,r_a.$$

When the number of temporal degrees-of-freedom is the same for each node in the element, i.e., $r_a = r,\ a = 1,\ldots,n_{en}$, then the approximation may be written as,

$$u(\boldsymbol{x},t) = \boldsymbol{N}^e(\boldsymbol{x}) \sum_{p=1}^{r} \boldsymbol{\phi}_p(t)\boldsymbol{d}(t_p) \qquad (20)$$

where, $\boldsymbol{\phi}(t) = \phi_p(t)\boldsymbol{I}_{n_{en}\times n_{en}}$, and $\boldsymbol{d}(t_p)$ is the vector, $\{u_a(t_p)\},\ a = 1,\ldots,n_{en}$. A similar approximation is given for the independent field variable $v(\boldsymbol{x},t)$ and auxiliary functions $\boldsymbol{w}(\theta,t)$.

Matrix Equations

Substituting the local space-time element approximations into (7), and after assembly, the space-time matrix equation for

each time slab takes the form,

$$\begin{bmatrix} \boldsymbol{K}_1 & -\boldsymbol{K}_2 \\ \boldsymbol{K}_2 & \boldsymbol{M}+\boldsymbol{C} \end{bmatrix} \begin{Bmatrix} \boldsymbol{u} \\ \boldsymbol{v} \end{Bmatrix} = \begin{Bmatrix} \boldsymbol{F}_u \\ \boldsymbol{F}_v \end{Bmatrix} \tag{21}$$

In the above, the global arrays are the assembly of space-time element matrices defined by,

$$\begin{aligned}
(\boldsymbol{m})_{e,i} &= [\boldsymbol{m}^{pq}] + [\delta_{1p}\delta_{1q}\delta_{1i}\boldsymbol{m}_e], \qquad \boldsymbol{m}^{pq} = \int_{I^e_{n,i}} \boldsymbol{\phi}_p^T(t)\boldsymbol{m}_e\dot{\boldsymbol{\phi}}_q(t)\,dt \\
(\boldsymbol{k}_1)_{e,i} &= [\boldsymbol{k}_1^{pq}] + [\delta_{1p}\delta_{1q}\delta_{1i}\boldsymbol{k}_e], \qquad \boldsymbol{k}_1^{pq} = \int_{I^e_{n,i}} \boldsymbol{\phi}_p^T(t)\boldsymbol{k}_e\dot{\boldsymbol{\phi}}_q(t)\,dt \\
(\boldsymbol{k}_2)_{e,i} &= [\boldsymbol{k}_2^{pq}], \qquad \boldsymbol{k}_2^{pq} = \int_{I^e_{n,i}} \boldsymbol{\phi}_p^T(t)\boldsymbol{k}_e\boldsymbol{\phi}_q(t)\,dt \\
(\boldsymbol{c})_{e,i} &= [\boldsymbol{c}^{pq}], \qquad \boldsymbol{c}^{pq} = \int_{I^e_{n,i}} \boldsymbol{\phi}_p^T(t)\boldsymbol{c}_e\boldsymbol{\phi}_q(t)\,dt
\end{aligned}$$

The space-time element force vectors are given by,

$$\begin{aligned}
(\boldsymbol{f}_u)_{e,i} &= \{\delta_{1p}\delta_{1i}\boldsymbol{k}_e\boldsymbol{d}(t_n^-)\} \\
(\boldsymbol{f}_v)_{e,i} &= \boldsymbol{f}_\Gamma + \boldsymbol{f}_S + \{\delta_{1p}\delta_{1i}\boldsymbol{m}_e\boldsymbol{v}(t_n^-)\}
\end{aligned}$$

with

$$\begin{aligned}
\boldsymbol{f}_\Gamma &= \{\boldsymbol{f}_\Gamma^p\}, \qquad \boldsymbol{f}_\Gamma^p = \sum_q \boldsymbol{k}_\Gamma^{pq}\boldsymbol{w}_{1,q}^e, \quad \boldsymbol{k}_\Gamma^{pq} = \int_{I^e_{n,i}} \boldsymbol{\phi}_p^T(t)\boldsymbol{k}_{\Gamma_e}\boldsymbol{\phi}_q(t)\,dt \\
\boldsymbol{f}_S &= \{\boldsymbol{f}_S^p\}, \qquad \boldsymbol{f}_S^p = \int_{I^e_{n,i}} \boldsymbol{\phi}_p^T(t)(N_a,\, f(\boldsymbol{x},t))_{\Omega_e}\,dt,
\end{aligned}$$

In the above, the spatial element mass, damping and stiffness matrices, are defined by standard L_2 inner products for a spatial element Ω_e and boundary element Γ_e

$$\begin{aligned}
\boldsymbol{m}_e &= [m_{ab}]_e, \qquad m_{ab} := \frac{1}{c^2}(N_a\,, N_b)_{\Omega_e}, \\
\boldsymbol{c}_e &= [c_{ab}]_{\Gamma_e}, \qquad c_{ab} := \frac{1}{c}(N_a\,, N_b)_{\Gamma_e}, \\
\boldsymbol{k}_e &= [k_{ab}]_e, \qquad k_{ab} := (\nabla N_a\,, \nabla N_b)_{\Omega_e} + \frac{1}{2R}(N_a\,, N_b)_{\Gamma_e} \\
\boldsymbol{k}_{\Gamma_e} &= [k_{ab}]_{\Gamma_e}, \qquad k_{\Gamma_e,ab} = (N_a\,, N_b)_{\Gamma_e}
\end{aligned}$$

The addition of standard mass and stiffness matrices $[\delta_{1p}\delta_{1q}\delta_{1i}\boldsymbol{m}_e]$ and $[\delta_{1p}\delta_{1q}\delta_{1i}\boldsymbol{k}_e]$ result from the jump terms appearing in the time-discontinuous variation equation at the beginning of the time slab. The Kronecker delta notation $\delta_{1p}\delta_{1q}\delta_{1i}$ indicates that they are assembled into the global matrices only at the beginning ($p = 1, q = 1$) of every 1st ($i = 1$) space-time element in the time direction. The size of the matrices are determined by the total number of degrees-of-freedom for the space time element, defined by $m = \sum_{a=1}^{n_{en}} r_a$.

The time integration is performed analytically in closed-form. Due to the assumed orthogonality of the space-time dimensions, when implemented at the component level, the element spatial matrix coefficients are independent of time allowing for simple time-integration of polynomial basis functions. For example, the components of the space-time mass matrix $\boldsymbol{m}^{pq}$ are computed from the integration of,

$$m_{ab}^{pq} = m_{ab}\int_{I^e_{n,i}} \phi_p(t)\dot{\phi}_q(t)\,dt$$

for $a, b = 1, \ldots, n_{en}$, $p = 1, \ldots, r_a$ and $q = 1, \ldots, r_b$.

While not required, for efficiency we assume that within a spatial element Ω_e, each sub-time step is the same size, i.e., $\Delta^e_{n,i} = \Delta^e_{n,1},\ i = 1, \ldots, N^e_t$, so that the space-time element matrices are computed once for all sub-time steps $I^e_{n,i}$, $i = 1, \ldots, N^e_t$.

The global matrices $\boldsymbol{K}_1$ and $\boldsymbol{M}$ are unsymmetric, while the coupling matrix $\boldsymbol{K}_2$ and damping matrix $\boldsymbol{C}$ is symmetric. This system is solved iteratively using the GMRES method with ILUT preconditioning.

Substitution of local space-time approximations into (8), the matrix equations for the nodal unknowns of the boundary auxiliary functions take the form,

$$(\boldsymbol{C}_w + \boldsymbol{K}_w)\boldsymbol{w} = \boldsymbol{F}_w \tag{22}$$

Boundary global matrices $\boldsymbol{C}_w$ and $\boldsymbol{K}_w$ and forcing vector $\boldsymbol{F}_w$ are formed by assembly of boundary space-time element array,

$$\boldsymbol{c}_w = [\boldsymbol{c}_w^{pq}] + [\delta_{1p}\delta_{1q}\delta_{1i}\boldsymbol{c}_w^e], \qquad \boldsymbol{c}_w^{pq} = \int_{I^e_{n,i}} \boldsymbol{\phi}_p(t)\,\boldsymbol{c}_w^e\,\dot{\boldsymbol{\phi}}_q(t)\,dt \tag{23}$$

$$\boldsymbol{k}_w = [\boldsymbol{k}_w^{pq}], \qquad \boldsymbol{k}_w^{pq} = \int_{I^e_{n,i}} \boldsymbol{\phi}_p(t)\,\boldsymbol{k}_w^e\,\dot{\boldsymbol{\phi}}_q(t)\,dt \tag{24}$$

$$\boldsymbol{f}_w = [\boldsymbol{f}_w^p] + \{\delta_{1p}\delta_{1i}\boldsymbol{c}_w^e\boldsymbol{w}(t_n^-)\}, \qquad \boldsymbol{f}_w^p = \sum_q \boldsymbol{k}_u^{pq}\boldsymbol{u}_{\Gamma,q}^e \tag{25}$$

where

$$\boldsymbol{k}_u^{pq} = \int_{I^e_{n,i}} \boldsymbol{\phi}_p(t)\,\boldsymbol{k}_u^e\,\boldsymbol{\phi}_q(t)\,dt.$$

In the above, spatial boundary element damping and stiff-

ness matrices are defined as

$$\boldsymbol{c}_w^e = [\boldsymbol{c}_{w,ab}]_e, \qquad \boldsymbol{c}_{w,ab} := \frac{1}{c}(N_a\,,N_b)_{\Gamma_e}\boldsymbol{I}$$

$$\boldsymbol{k}_w^e = [\boldsymbol{k}_{w,ab}]_e, \qquad \boldsymbol{k}_{w,ab} := \frac{1}{4R}(N_a\,,N_b)_{\Gamma_e}\boldsymbol{A}_1 - \frac{1}{4R}(\frac{\partial N_a}{\partial\theta}\,,\frac{\partial N_b}{\partial\theta})_{\Gamma_e}\boldsymbol{A}_2$$

with boundary element force vector,

$$\boldsymbol{f}_w^e = \{\boldsymbol{f}_{w,a}\}_e, \quad \boldsymbol{f}_{w,a} := \sum_{b=1}^{n_{en}} k_{u,ab}\,u_{\Gamma,b}\,\boldsymbol{e}_1$$

$$\boldsymbol{k}_u^e = [k_{u,ab}], \quad k_{u,ab} := (N_a\,,N_b)_{\Gamma_e}b_1 - (\frac{\partial N_a}{\partial\theta}\,,\frac{\partial N_b}{\partial\theta})_{\Gamma_e}b_2$$

These boundary element arrays can be computed in closed-form, for details see [16]. The force vector is coupled to the field solution evaluated on the boundary $\boldsymbol{u}_\Gamma$.

A multi-level iterative method is used to solve the coupled interior and boundary equation system defined by (21) and (22). A restarted version of Generalized Minimal Residual (GMRES) method with ILUT preconditioner is used to solve both the interior and boundary equation systems. An outer iterative loop is used around the interior and boundary equation solvers to obtain converged solutions for the coupled system.

LOCAL ADAPTIVE STRATEGY

When using different numbers of sub-time steps for different elements, the temporal error estimator used in [9], [11]- [13], [14], based on the jump terms at the beginning of a global time slab, cannot be used to predict new sub-time step sizes. For this reason, new temporal error estimators are developed for the TDG FEM with continuous local temporal adaptivity within a space-time slab.

Temporal Error Estimators

For time slab n, the total energy norm is the summation of energy over each spatial element in the computational domain,

$$||\boldsymbol{u}||_n^2 = \sum_e ||\boldsymbol{u}^e||_n^2 \tag{26}$$

The total energy over each element in a time-slab is obtained by adding contributions from each sub-time step for that element,

$$||\boldsymbol{u}^e||_n^2 = \frac{1}{\Delta t_n}\sum_{i=1}^{N_t^e}\int_{I_{n,i}^e}\{\boldsymbol{u}(t)\cdot\boldsymbol{k}_e\boldsymbol{u}(t) + \boldsymbol{v}(t)\cdot\boldsymbol{m}_e\boldsymbol{v}(t)\}\;\mathrm{d}t \tag{27}$$

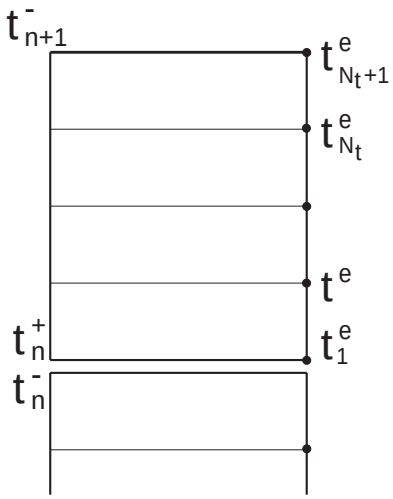

Figure 4. Illustration of local sub-time step numbers used for temporal error estimation.

Figure 4 shows an illustration of local sub-time steps used in the summation. Here $\boldsymbol{u}(t)$ and $\boldsymbol{v}(t)$ are the time-dependent solution vectors of dimension equal to the number of spatial element nodes. The estimated temporal error for each spatial element measured in the energy norm can be written as

$$\begin{aligned}||\boldsymbol{e}_t^*||_e^2 &= \frac{1}{\Delta t_n}\int_{I_n}\{\boldsymbol{e}_u^*(t)\cdot\boldsymbol{k}_e\boldsymbol{e}_u^*(t) + \boldsymbol{e}_v^*(t)\cdot\boldsymbol{m}_e\boldsymbol{v}_v^*(t)\}\;\mathrm{d}t \\ &= \frac{1}{\Delta t_n}\sum_{i=1}^{N_t^e}\int_{I_{n,i}^e}\{\boldsymbol{e}_u^*(t)\cdot\boldsymbol{k}_e\boldsymbol{e}_u^*(t) + \boldsymbol{e}_v^*(t)\cdot\boldsymbol{m}_e\boldsymbol{v}_v^*(t)\}\;\mathrm{d}t\end{aligned} \tag{28}$$

where $\boldsymbol{e}_u^*(t)$ and $\boldsymbol{e}_v^*(t)$ are error estimates for the field variables in each element.

The estimated total temporal error for the time step n is then the summation over all elements,

$$||\boldsymbol{e}_t^*||_n^2 = \sum_e ||\boldsymbol{e}_t^*||_e^2 \tag{29}$$

Three alternative recovery based error indicators are developed to drive the local sub-time step adaptive process.

$$\begin{array}{lll}\text{I.} & e_v^* = v^h - \frac{du^h}{dt}, & e_u^* = 0 \\ \text{II.} & e_v^* = (\frac{du}{dt})^* - \frac{du^h}{dt}, & e_u^* = 0 \\ \text{III.} & e_v^* = v^* - v_h, & e_u^* = u^* - u_h\end{array}$$

Each of these three temporal error indicators are compared numerically in [23].

Temporal Error Estimate I

Taking advantage of the dual-field space-time formulation, for a spatial node within a sub-time step, we define the error indicator from,

$$e_v^* = v^h - \frac{du^h}{dt}, \qquad e_u^* = 0$$

The independent field variable v^h is one order higher more accurate than the derivative du^h/dt. Then this error estimate is asymptotically optimal. The temporal convergence rate is dictated by the temporal gradient du^h/dt, so that $e_u^* = u^* - u^h \ll e_v^* \Rightarrow e_u \approx 0$, and with sufficient regularity, the convergence rate is, $||\boldsymbol{e}_t^*||_n \sim O(\Delta t_n^p)$, where p is the polynomial order in the temporal approximation. For example, space-time elements with linear polynomial approximation in time, within each sub-time step, v^h varies linearly while du^h/dt is a constant, and $||\boldsymbol{e}_t^*||_n \sim O(\Delta t_n^1)$.

Temporal Error Estimate II

Based on a superconvergent patch recovery (SPR) of sub-time step nodes, the error can be estimated from

$$e_v^* = (\frac{du}{dt})^* - \frac{du^h}{dt}, \qquad e_u^* = 0$$

Here $(du/dt)^*$ is the more accurate gradient recovered from a one-dimensional superconvergent patch recovery in the time-dimension of the discontinuous finite element temporal gradients du^h/dt. For improved accuracy we form a patch for each node $(\boldsymbol{x}_A, t_n^+)$ at the beginning of a current time slab, we use $(\boldsymbol{x}_A, t_n^- - \Delta t_{n-1}^A)$; where Δt_{n-1}^A is the sub-time step size at node x_A in the previous time slab. Using this measure, the convergence rate is, $||\boldsymbol{e}_t^*||_n \sim O(\Delta t_n^p)$. For linear polynomials in time, $p = 1$.

Temporal Error Estimate III

Based on the superconvergent interpolation (SI) method derived in [14], here applied for temporal error estimation. With improved temporal derivatives by SPR, use one-dimensional SI method to obtain improved solutions $u^*(\boldsymbol{x},t)$ and $v^*(\boldsymbol{x},t)$ within each sub-time step. Define the estimated displacement and velocity errors as

$$e_u^* = u^* - u_h, \qquad e_v^* = v^* - v_h$$

Using this measure, the convergence rate is, $||\boldsymbol{e}_t^*||_n \sim O(\Delta t_n^{p+1})$.

Adaptive Sub-time Step Size and Distribution

To maintain a specified level of accuracy at a given time step, the estimated temporal relative error is enforced to be below a specified tolerance:

$$\eta_t = \frac{||\boldsymbol{e}_t^*||_n}{||\boldsymbol{u}^h||_n} \le \eta_t^{TOL} \tag{30}$$

If $\eta_t > \eta_t^{TOL}$, a new time slab with new global time step size and sub-time step distribution is needed. In order to obtain an optimal distribution, the temporal error is uniformly redistributed. A temporal error density $\bar{e}$ (temporal error per unit area) is defined to quantify the uniformity of the distributed temporal error. An optimal mesh implies a uniform distribution of the error density. For current time slab n, we define the permissible error density tolerance over the total computational domain Ω, as

$$\bar{e}^{TOL} = \frac{\eta_t^{TOL}||u^h||_n}{\sqrt{A_\Omega}} \tag{31}$$

where A_Ω is the total area of the computational domain Ω.

To obtain uniformly distributed temporal error, the permissible temporal error for element Ω_e is set to be $\sqrt{A_e}\bar{e}^{TOL}$, where A_e is the area of element Ω_e. Based on the convergence rate for norm I and II, $\|\boldsymbol{e}_t^*\|_e \sim O(\Delta t_e^p)$, where $\Delta t_e = \Delta t_n^e$ is the sub-time step size for element Ω_e, a new optimal sub-time step size $\Delta t_e'$ for each element can be predicted from,

$$\Delta t_e' = \frac{\Delta t_e}{\xi_e}, \qquad \xi_e = \left(\frac{||e_t^*||_e}{\sqrt{A_e}\bar{e}^{TOL}}\right)^{1/p} \tag{32}$$

where Δt_e is the old sub-time step size for this element, and ξ_e is the refinement parameter. In practice, it is not possible to use this optimal time step since the sub-time steps are assumed equally spaced for simplicity and must add up to the total time-slab size for all elements in the space-time mesh. For norm III, $p \to p+1$.

The optimal new sub-time step distribution is approximated using the following strategy. The idea is to find a minimum new sub-time step size for the new time slab n, denoted $\Delta t_{min}'$, based on an average time-step from an equivalent single-step time slab. The new sub-time steps for each spatial element are determined by comparing the predicted values from (32) within finite intervals defined by multiples of the minimum time step, e.g. $\Delta t_{min}', 2\Delta t_{min}', 4\Delta t_{min}', \ldots$.

An average global time step size $\Delta\bar{t}$, is determined by converting the current time slab into an approximately equivalent slab with the same temporal error and only one sub-time step everywhere. Based on the order of accuracy $\|\boldsymbol{e}_t^*\|_e^2 \sim O(\Delta t_e^{2p})$, and

equating the total estimated temporal error with the total temporal error for an equivalent slab with only one sub-time step everywhere, we have

$$||\boldsymbol{e}_t^*||_n^2 \simeq \sum_e \left(\frac{\Delta\bar{t}}{\Delta t_e}\right)^{2p} ||\boldsymbol{e}_t^*||_e^2 \tag{33}$$

then the average time step size is approximated as,

$$\Delta\bar{t} \simeq \frac{(||\boldsymbol{e}^*{}_t||_n)^{1/p}}{\xi}, \qquad \xi = \left(\sum_e \frac{||\boldsymbol{e}_t^*||_e^2}{(\Delta t_e)^{2p}}\right)^{1/2p} \tag{34}$$

To satisfy the required tolerance η_t^{TOL}, the new average time step size would be

$$\Delta\bar{t}' = \left(\frac{\eta_t^{TOL}}{\eta_t}\right)^{1/p} \Delta\bar{t} \tag{35}$$

The new minimum sub-time step size is then defined by a fraction of this average time step size, $\Delta t'_{min} = \gamma_t \Delta\bar{t}'$ Here $\gamma_t < 1$ is a parameter used to control the sub-time step distribution. Numerical studies given in [23] show that the efficiency of the temporal error distribution is relatively insensitive to the exact choice for the parameter γ_t.

The prescribed maximum number of sub-time steps for each time slab is set to be $N_{max} = 2^{K_t}$, $K_t = 0,1,2,\ldots$, resulting in a global time slab size $\Delta t_n = N_{max}\Delta t'_{min}$ For each element, if the predicted sub-time step size computed in (32) satisfies

$$\begin{array}{llll}
\text{If} & (0 < \Delta t'_e < \Delta t'_{min}), & \text{Set:} & k_e = 0 \\
\text{If} & (2^0\Delta t'_{min} \le \Delta t'_e < 2^1\Delta t'_{min}), & \text{Set:} & k_e = 1 \\
 & \vdots & \vdots & \vdots \\
\text{If} & (2^{K_t-2}\Delta t'_{min} \le \Delta t'_e < 2^{K_t-1}\Delta t'_{min}), & \text{Set:} & k_e = K_t - 1 \\
\text{If} & (2^{K_t-1}\Delta t'_{min} \le \Delta t'_e), & \text{Set:} & k_e = K_t
\end{array}$$

The number of sub-time steps for this element is $N_t^e = 2^{K_t - k_e}$, while the new adjusted sub-time step size is then

$$\Delta t'_e = 2^{k_e}\Delta t'_{min} \tag{36}$$

With new sub-time step sizes adjusted in (36), $\Delta t'_{min}$ also needs to be adjusted to ensure the new temporal relative error η_t satisfies the tolerance η_t^{TOL}. Based on the order of accuracy $\|\boldsymbol{e}_t^*\|_e^2 \sim O((\Delta t_e)^{2p})$, and $\|\boldsymbol{e}'_t\|_e^2 \sim O((\Delta t'_e)^{2p})$ the new temporal error is estimated from,

$$||\boldsymbol{e}'_t||_n^2 = \sum_e ||\boldsymbol{e}'_t||_e^2 = \sum_e \left(\frac{\Delta t'_e}{\Delta t_e}\right)^{2p} \|\boldsymbol{e}_t^*\|_e^2$$

Then the new minimum sub-time step size which will result in the tolerance being satisfied is determined from,

$$\Delta t_{min} = \frac{\Delta t'_{min}}{\xi_t}, \quad \text{with } \xi_t = \left(\frac{||\boldsymbol{e}'_t||_n}{\eta_t^{TOL}\|u\|_n}\right)^{1/p}$$

Finally, for each spatial element, the new sub-time step size is now $\Delta t_e^{new} = 2^{k_e}\Delta t_{min}$, and the global time slab size is $\Delta t_n = N_{max}\Delta t_{min}$.

For example, with $N_{max} = 4$, the adaptive distribution of local sub-time step sizes for each element will fall into the following categories $\Delta t_{min} = \Delta t_n/4, 2\Delta t_{min} = \Delta t_n/2, 4\Delta t_{min} = \Delta t_n$, where Δt_n is the adaptive global time-slab size.

Local Temporal Basis Functions

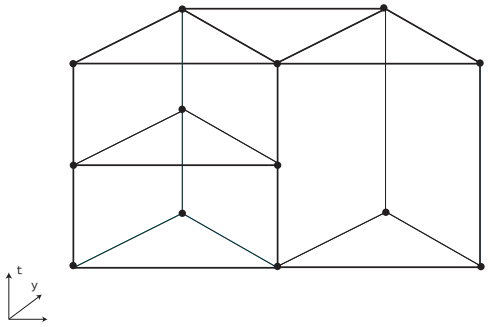

Figure 5. Combination of three different kinds of elements showing transition of two sub-time steps for the element on the left to adjacent elements with one time step. The two elements with no transition nodes on the left have one-half the sub-time step size, as the two transition elements; the center element with two transition edges, and the element on the right with one transition edge.

Although not required, in order simplify the adaptive solution within a space-time slab, the following restrictions on the division of sub-time steps are followed.

- Orthogonal space-time elements; the time direction of each element is perpendicular to the spatial dimensions.
- Piecewise linear basis functions in the time dimension are used for all elements within a space-time slab.
- Permissible sub-time steps and sizes to increase by order two.
- Transition elements with hanging nodes at the middle points of temporal edges introduced to maintain continuity of solutions across space-time elements within a time-slab.

An illustrative space-time mesh with these assumptions is shown in Figure3.

As stated earlier, within a space-time element $\Omega_n^e \times I_{n,i}^e$, the solution is interpolated in time using,

$$u(\boldsymbol{x},t) = \sum_{a=1}^{n_{en}} N_a(\boldsymbol{x}) u_a(t), \quad \text{where } u_a(t) = \sum_{p=1}^{r_a} \phi_{a,p}(t) u_a(t_p)$$

Here r_a is the number of temporal nodes at spatial node a within a sub-time step. A linear temporal interpolation is employed with standard Lagrange basis functions $\phi_{a,p}(t)$. Using a standard linear mapping

$$t = \frac{t_1+t_2}{2} + \frac{\tau}{2}(t_2-t_1), \quad t_1 = t_{n,i}^e, \; t_2 = t_{n,i+1}^e$$

with the jacobian $dt/d\tau = \Delta t_{n,i}^e/2$. The basis functions associated with the beginning and end of a sub-time step interval at a typical node a are defined by,

$$\phi_{a,p}(\tau) = \frac{1}{2}(1+\tau_p\tau), \quad p = 1,2, \quad \text{where} \quad (\tau_1,\tau_2) = (-1,1)$$

To maintain continuity across adjacent elements with smaller (by 1/2) sub-time step sizes, a transition node is introduced at the middle point of the temporal edge. In this case the following piecewise linear shape functions are used,

$$\phi_{a,p}(\tau) = \begin{cases} (1-\delta_{p2})(\delta_{p3}(1+\tau)+\tau_p\tau) \;, \; \tau \le 0; \\ (1-\delta_{p1})(\delta_{p3}(1-\tau)+\tau_p\tau) \;, \; \tau > 0. \end{cases}$$

with $p = 1,2,3$, and $(\tau_1,\tau_2,\tau_3) = (-1,1,0)$.

The space-time element is defined by the temporal projection of a spacial element. For problems in two-spatial dimensions, the space-time element defined by the temporal projection of a standard 3-node linear triangle element can be visualized as a three-dimensional wedge. To maintain mesh continuity, three possible kinds of space-time elements are developed, see Figure (5). The first is a standard space-time wedge element with no transition nodes. Two possible transition elements are possible; elements with one transition node on an edge, and elements with two transition nodes, one on each edge.

By maintaining orthogonality of the space-time mesh and pre-integrating analytically through the time-slab, we obtain an efficient yet robust adaptive method where any standard spatial element may be used with no modifications. The procedures have been implemented in two- spatial dimensions with linear interpolations, but the procedures are valid for three-dimensions and higher-order interpolations as well, including hp-meshes, with combinations of low-order and high-order space-time interpolations.

Spatial Error Estimation

In this work, we use *h*-adaptive solution methods with unstructured spatial meshes. Other spatial adaptive schemes may also be used, including *hp*-adaptive meshes. For an estimate of the spatial error at a given global time-step, we compute the difference between superconvergent patch recovery (SPR) gradients ∇u^*, [17], and constant finite element gradients ∇u^h measured in the L_2 norm. The error is computed over each element Ω_e, and summed to give the global error,

$$||\boldsymbol{e}_s||_n^2 = \sum_{e=1}^{ne} ||\boldsymbol{e}_s||_{n,e}^2 \tag{37}$$

$$||\boldsymbol{e}_s||_{n,e}^2 = \int_{\Omega_e} [\nabla u^*(\boldsymbol{x},t_{n+1}^-) - \nabla u^h(\boldsymbol{x},t_{n+1}^-)]^2 \, \mathrm{d}\boldsymbol{x}$$

Since the recovered gradient ∇u^* converges at a higher rate than the FEM gradient ∇u^h, the effectivity of the error indicator is asymptotically exact.

To control the spatial accuracy, the estimated relative error is kept below a specified tolerance:

$$\eta_s(t_n) = \frac{||\boldsymbol{e}_s||_n}{||u^h||_n} \le \eta_s^{TOL} \tag{38}$$

Once the estimated error is calculated, and it is determined that a new mesh is required, an optimal mesh is obtained by assuming equal distribution of error with the least number of required elements. The refinement condition which satisfies this optimal criteria is determined from,

$$h_e^{new} = h_e^{old}/\xi_e \tag{39}$$

where h_e^{old} denotes the characteristic size of element e, in the previous (old) mesh, and h_e^{new} is the desired size of the new elements in the region covered by that old element. The refinement parameter is defined on each element by [18]:

$$\xi_e = \frac{\eta_e^{1/(p+1)}}{(\eta_s^{TOL})^{1/p}} \left[\sum_{e=1}^{N_e} \eta_e^{2/(p+1)} \right]^{1/2p}, \qquad \eta_e = \frac{||\boldsymbol{e}_s||_{n,e}}{||u^h||_{n,e}} \tag{40}$$

In the above, p is the polynomial degree of the basis functions used in the spatial mesh, and η_e is the contribution from element e to the estimated relative global error, η_s.

Superconvergent Interpolation

For adaptive meshes, the solution at a global time-step must be transferred from the old mesh to the new mesh. For low-order elements in space, standard nodal interpolation may introduce significant accumulation of error. To correct this problem, we have developed a new *superconvergent interpolation* scheme [14]. Prior to projecting, the solution on the top of previous time-slab, $t_{n-1}^{+} = t_n^{-}$, is interpolated with,

$$u(\boldsymbol{x}, t_n^-) = \sum_{a=1}^{\text{nnodes}} N_a^-(\boldsymbol{x}) \left[u_a^h(t_n^-) + \hat{\boldsymbol{x}}_a \cdot \nabla u_a^*(\boldsymbol{x}_a^c, t_n^-) \right] \qquad (41)$$

where, $\hat{\boldsymbol{x}}_a = \boldsymbol{x} - \boldsymbol{x}_a$, and the vector, $\nabla u_a^*(\boldsymbol{x}_a^c, t_n^-)$ is the recovered gradients obtained by superconvergent patch recovery (SPR) at node a, evaluated at the midpoint between node $\boldsymbol{x}_a$, and position $\boldsymbol{x}$. A similar technique is used for $v(\boldsymbol{x}, t_n^-)$. This scheme may be viewed as a correction to standard interpolation, and provides significantly improved accuracy. Extensions to tetrahedron elements is straightforward.

NUMERICAL EXAMPLE

An illustrative example of our local space-time adaptive solution strategy is presented for the problem of radiation from a line element on a circle, driven by a modified Ricker pulse [21]. Details for this problem are given in [14]. The ratio of the inner radiating circle of radius a to the outer artificial truncation boundary is fixed at $R/a = 1.75$ The local radiation boundary conditions are employed on the encircling truncation boundary with a total of $p = 3$ auxiliary boundary functions; previous studies for this example problem have shown that this number is sufficient for a highly accurate non-reflecting boundary.

Results are shown with the relative temporal error measured in norm II controlled by a tolerance of $\eta_t = 4\%$. The minimum sub-time step size distribution parameter defined in () is set at $\gamma_t = 0.4$. The maximum allowed sub-time step number is $N_{max} = 4$, resulting in either 1, 2 or 4 sub-time steps per spatial element. The initial spatial mesh has 3400 three-node triangle elements resulting in 1806 nodes. The adaptive mesh is controlled by a a spatial error norm maintained below $\eta_s = 10\%$.

Figure 6 shows the contours for the field solution $u(\boldsymbol{x}, t)$ at representative snapshots in time t. For ease of visualization, the contours are rescaled at each time step, so that the max/min values at a given time step are distributed evenly between twenty contour lines. The initial wave-front reaches the truncation boundary at $t = c(R-a) = 0.375$. Examining the time-history of the total energy norm within the computational domain Ω, most of the radiated energy has left the computational domain after $t = 1$. Figure 7 shows the adaptive mesh tracking the wave pulse through the computational domain. Figure 8 and Figure 9 shows the corresponding temporal error estimation

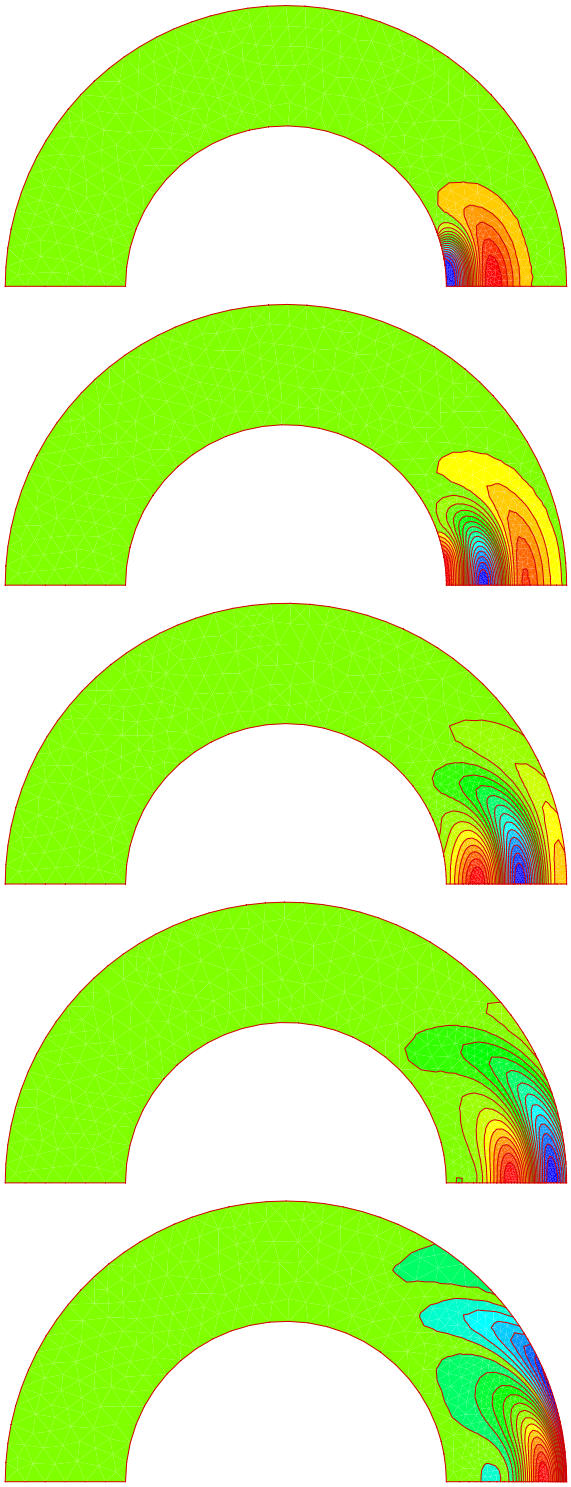

Figure 6. Solution contour at snapshots in time between $t = (0.4, 0.8)$.

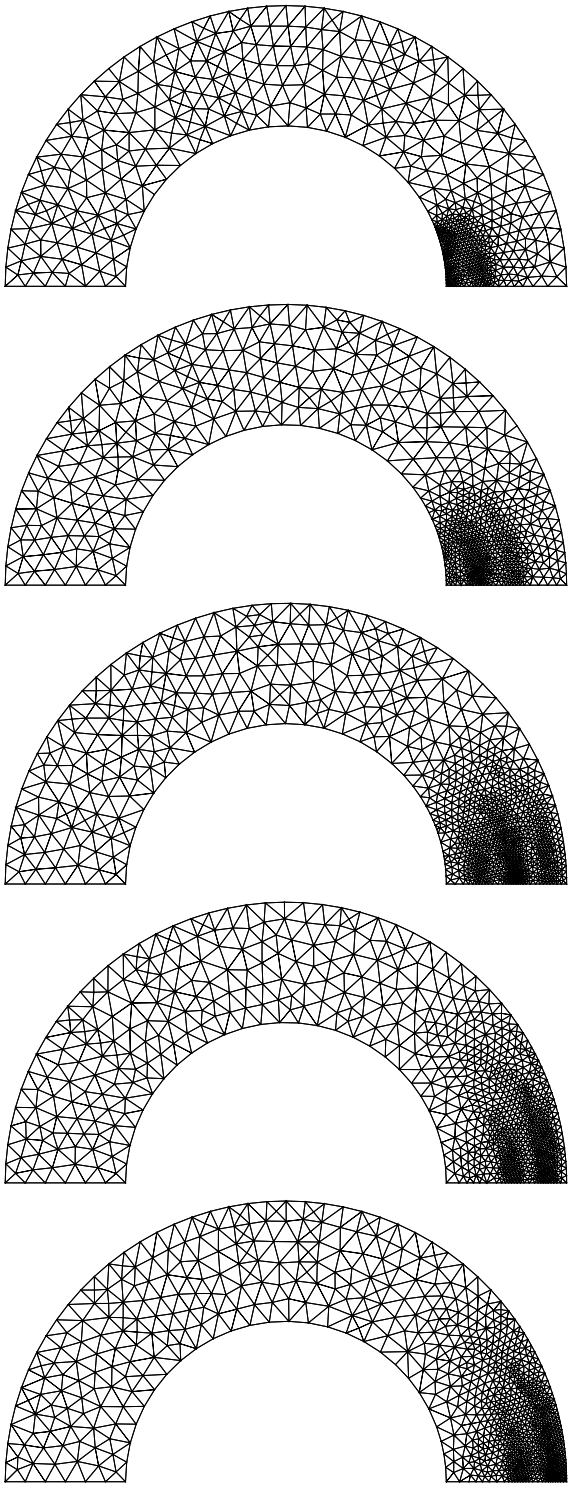

Figure 7. Adaptive mesh at snapshots in time between $t = (0.4, 0.8)$.

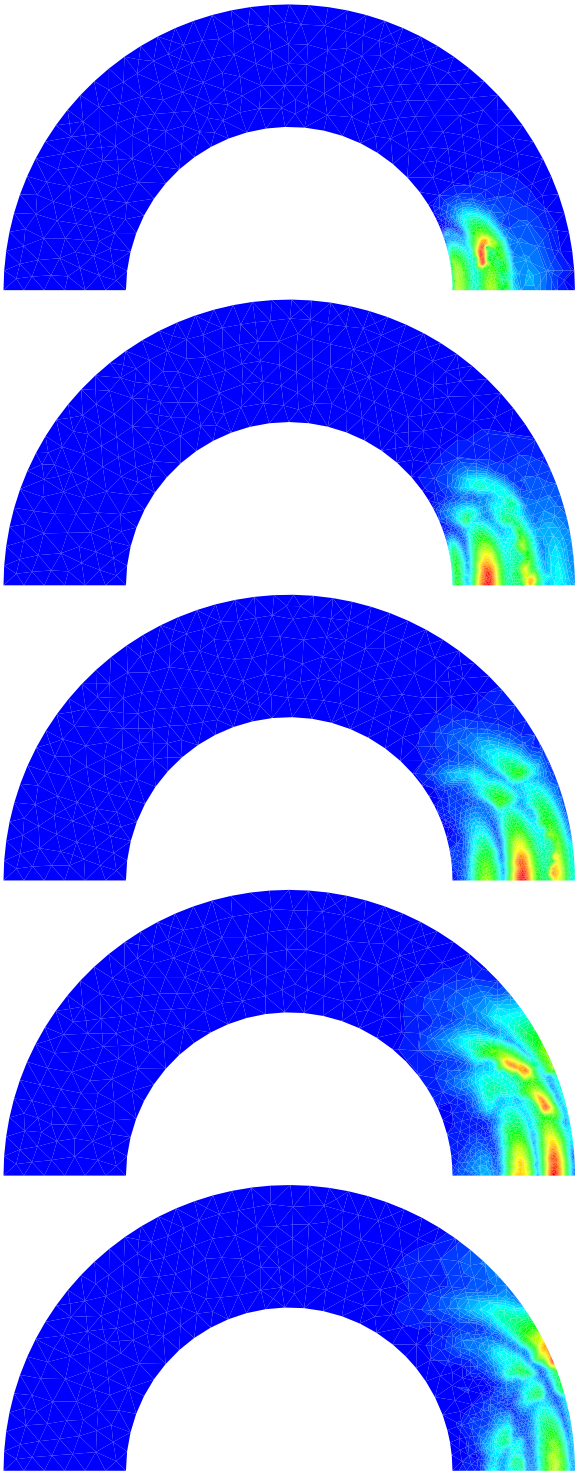

Figure 8. Temporal error norm II, with $\gamma_t = 0.4$. Estimated temporal error with adaptive global time-slab size Δt_n and adaptive distribution of local sub-time step sizes $\Delta t_{min} = \Delta t_n/4, 2\Delta t_{min} = \Delta t_n/2, 4\Delta t_{min} = \Delta t_n$.

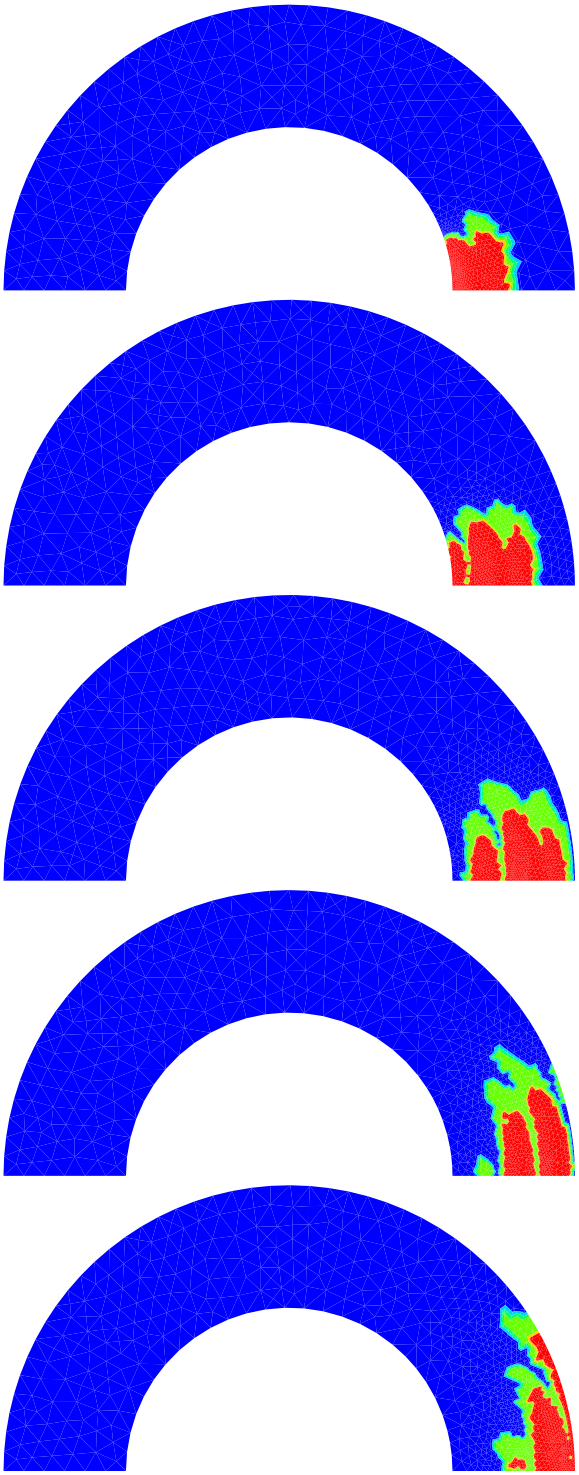

Figure 9. Temporal error norm II, with $\gamma_t = 0.4$. Adaptive sub-time step distribution with sub-time step sizes: (Red) $\Delta t_n/4$; (Green) $\Delta t_n/2$; (Blue) Δt_n

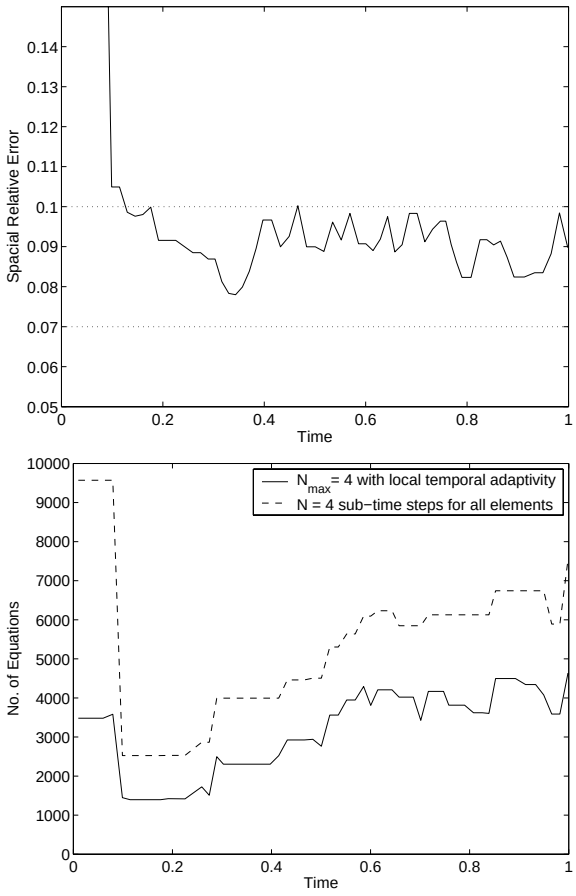

Figure 10. (Top) Relative spatial error controlled by tolerance, $\eta_s^{TOL} = 10\%$, and parameters $(\beta_{s1}, \beta_{s2}) = (0.5, 1.15)$, $K_t = 20$. (Bottom) Number of equations in the corresponding adaptive mesh. The results show a significant reduction in the number of equations within a space-time slab with local adaptive sub-time steps compared to a uniform distribution of sub-time steps.

and resulting local sub-time step distributions, respectively. Both spatial element and sub-time step distributions are seen to track the solution well.

Figure 10 (Top) shows the estimated relative spatial error is controlled to be below the tolerance $\eta_s = 10\%$. The mesh is re-distributed to maintain the specified error tolerance. Figure 10 (Bottom), compares the number of space-time equations within a space-time slab using local adaptive sub-time step distributions with $N_{max} = 4$ with the number of space-time equations required if a constant time-step distribution is used with the minimum sub-time step size and $N = 4$ sub-time steps for each spatial element. It can be seen that by using local temporal adaptivity, a significant reduction in the number of equations within a space-time slab is achieved compared to a uniform distribution of sub-time steps.

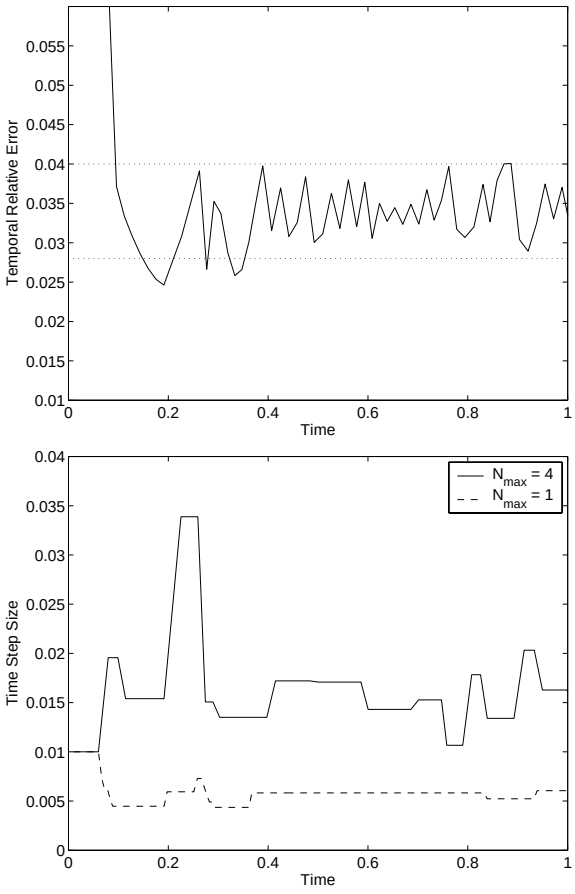

Figure 11. (Top) Relative temporal error controlled by parameters, $\eta_t^{TOL} = 4\%$, $(\beta_{t1}, \beta_{t2}) = (0.7, 1.2)$, $K_t = 10$. (Bottom) Corresponding adaptive global time-step sizes.

Figure 11 shows the relative temporal error estimate based on norm II as a function of time with the corresponding global time slab size change. The global time-step size and sub-time step distribution is changed such that the error tolerance is satisfied. The plot also compares the time step sizes with $N_{max} = 4$ and $N_{max} = 1$. For the case of $N_{max} = 4$, local temporal adaptivity provides for different sub-time step sizes for different spatial elements. For the case $N_{max} = 1$, global temporal adaptivity is performed with each element having the same time-step size. The results demonstrate that our local temporal adaptive strategy allows for much larger time slab sizes to achieve the same required temporal relative error.

CONCLUSIONS

We have proposed a new local adaptive space-time finite element strategy for solving second-order hyperbolic systems. The methods are demonstrated for the scalar wave equation governing time-dependent acoustic waves, but also are applicable to other systems including elastodynamics and other wave problems. The time-discontinuous Galerkin (TDG) variational method is used to divide the time-interval into space-time slabs, the solution advanced from one slab to the next, similar to standard time-stepping methods. Within each slab, a continuous space-time mesh is used. By maintaining orthogonality of the space-time mesh and pre-integrating analytically in the time-dimension through each local element in the time-slab, we obtain an efficient yet robust adaptive method where any standard spatial element may be used with no modifications; for example for structural acoustics applications standard acoustic and shell elements may be used. No complicated 4-dimensional unstructured space-time mesh generation and visualization schemes are required. The methods are implemented in two spatial dimensions with linear interpolations, but the procedures are valid for three spatial dimensions and higher-order interpolations as well. As far as we know, our new temporal error indicators to adaptively distribute local sub-time steps in different elements, together with synchronized global step sizes, are the first use of superconvergent recovery-based procedures for finite elements in the time-dimension.

In summary, the new ideas developed in this work are:

- Use the time-discontinuous Galerkin method to divide the time interval into time slabs, but allow for local continuous space-time elements within each slab.
- Restrict the time-edge of local space-time elements to be orthogonal to the space dimension so that the time integration is analytically evaluated in closed-form and decoupled from the space integration. The advantage is that any standard spatial element may be used with no modification, providing an efficient yet robust adaptive methodology; special 4-dimensional space-time elements requiring complicated formulations, mesh generation and visualization are not required.
- Recovery based error estimators such as the superconvergent patch recovery methods (SPR) commonly used for spatial meshes, may be used to compute effective temporal error estimates for adaptive space-time meshes.
- An adaptive strategy combining local spatial meshes together with local time-steps within space-time slabs using the TDG space-time finite element method provides an accurate, reliable, and efficient solution procedure for modeling localized wave problems over large distances and time.

These ideas were first presented in [22]. Further details and extensive numerical studies are found in [23].

ACKNOWLEDGMENT

Support for this work was provided by the National Science Foundation under Grant CMS-9702082 in conjunction with

a Presidential Early Career Award for Scientists and Engineers (PECASE), and is gratefully acknowledged.

REFERENCES

[1] T.J.R. Hughes, Hulbert, G., 'Space-time finite element methods for elastodynamics: Formulations and error estimates', *Computer Methods in Applied Mechanics and Engineering*, **66**, 339-363, 1988.

[2] C. Johnson, 'Discontinuous Galerkin finite element methods for second order hyperbolic problems', *Computer Methods in Applied Mechanics and Engineering*, **107**, 117-129, 1993.

[3] L.L., Thompson, P.M. Pinsky, 'A Space-time finite element method for structural acoustics in infinite domains, Part I: Formulation, Stability, and Convergence', *Computer Methods in Applied Mechanics and Engineering*, **132**, pp. 195-227, 1996.

[4] L.L., Thompson, P.M. Pinsky, 'A Space-time finite element method for structural acoustics in infinite domains, Part II: Exact time-dependent non-reflecting boundary conditions', *Computer Methods in Applied Mechanics and Engineering*, **132**, pp. 229-258, 1996.

[5] L.L. Thompson, P.M. Pinsky, 'A Space-time finite element method for the exterior structural acoustics problem: Time-dependent radiation boundary conditions in two spatial dimensions', *International Journal for Numerical Methods in Engineering*, **39**, pp. 1635-1657, 1996.

[6] L.L. Thompson, P.M. Pinsky, 'A space-time finite element method for the exterior acoustics problem', *Journal of the Acoustical Society of America*, **99** (6), pp. 3297-3311, 1996.

[7] L.L. Thompson, 'A multi-field space-time finite element method for structural acoustics', *Proceedings of the 1995 Design Engineering Technical Conferences, Acoustics, Vibrations, and Rotating Machines*, Vol. 3, Part B, ASME, pp. 49 - 64, Boston, Mass., Sept. 17-21, 1995.

[8] L.L. Thompson, 'Advances in Space-Time Finite Element Methods for Structural Acoustics and Fluid-Solid Interaction', *Proceedings of the Second International Conference on Theoretical and Computational Acoustics*, Honolulu, Hawaii, 21-25, August 1995. D. Lee, Y-H Pao, M.H. Schultz, and Y-C Teng (Editors), World Scientific Publishing Co., pp. 223-234, 1996.

[9] N-E Wiberg, X.D. Li, 'Adaptive finite element procedures for linear and non-linear dynamics', *International Journal for Numerical Methods in Engineering*, **46**, 1781-1802, 1999.

[10] C.C. Chien, T.Y. Wu, 'An improved predictor/multi-corrector algorithm for a time-discontinuous Galerkin finite element method in structural dynamics', *Computational Mechanics*,**25**, 430-437, 2000.

[11] L.L. Thompson, D. He; 'Adaptive space-time finite element methods for time-dependent acoustic scattering', Proceedings of USACM Sixth U.S. National Congress on Computational Mechanics, Deerborn, Michigan, July 31-Aug 4, 2001.

[12] L.L. Thompson, D. He; 'Adaptive space-time finite element methods for acoustics simulations in unbounded domains', Proceedings of Forum Acusticum Sevilla 2002, Sevilla, Spain, Sept. 16-20, 2002.

[13] L.L. Thompson, D. He; 'Adaptive time-discontinuous Galerkin methods for acoustic scattering in unbounded domains', Proceedings of 2002 ASME International Mechanical Engineering Congress and Exposition, Paper No. IMECE2002/NCA-32737, Nov. 17-22, 2002, New Orleans, Louisiana.

[14] Thompson, L.L., Dantong He, "Adaptive space-time finite element methods for the wave equation on unbounded domains", To Appear *Comput. Methods in Appl. Mech. Engrg*.

[15] T. Hagstrom and S. Hariharan, 'A formulation of asymptotic and exact boundary conditions using local operators', *Appl. Num. Math.* **27**, 403-416, 1998.

[16] L.L. Thompson, R. Huan, D. He, 'Accurate radiation boundary conditions for the two-dimensional wave equation on unbounded domains', *Computer Methods in Applied Mechanics and Engineering*, 191 (2001) 311-351.

[17] O. C. Zienkiewicz, J. Z. Zhu, 'The superconvergent patch recovery and a posterior error estimates. Part 1: The Recovery technique', *International Journal for Numerical Methods in Engineering*, Vol.**33**, 1331-1364, 1992.

[18] P. Coorevits, P. Ladeveze, J.P. Pelle, 'An automatic procedure with a control of accuracy for finite element analysis in 2D elasticity', *Computer Methods in Applied Mechanics and Engineering*, **121**, 91-120, 1995.

[19] Y.Saad and M.H. Schultz. 'GMRES: a generalized minimal residual algorithm for solving nonsymmetric linear systems. *SIAM Journal on Scientific and Statistical Computing*, 7:856-869, 1986.

[20] Yousef Saad, *Iterative methods for sparse linear systems*, PWS Publishing Company, 1996.

[21] N. H. Ricker, Transient Waves in Visco-Elastic Media, Elsevier, Amsterdam, Netherlands, 1977.

[22] He, D. and Thompson, L.L., "Adaptive time-discontinuous Galerkin finite element methods for acoustic scattering", *145th meeting of the Acoustical Society of America*, Session 3aSAb: Structural Acoustics and Vibration: Computational Methods, Nashville, Tennessee, April 28 – May 2, 2003. Abstract 3aSAb1, J. Acoust. Soc. Am., Vol. 113, No. 4, Pt. 2, April 2003, page 2252.

[23] He, Dantong. , "Local Space-Time Adaptive Finite Element Methods for the Wave Equation on Unbounded Domains", Ph.D. Dissertation, Clemson University (May 2003).